

MambaNet: Mamba-assisted Channel Estimation Neural Network With Attention Mechanism

Dianxin Luan*, Chengsi Liang†, Jie Huang‡§, Zheng Lin¶, Kaitao Meng||, John Thompson* and Cheng-Xiang Wang‡§

* Institute for Imaging, Data and Communications, School of Engineering, University of Edinburgh, Edinburgh, UK

† James Watt School of Engineering, University of Glasgow, Glasgow, UK

‡ National Mobile Communications Research Laboratory, Southeast University, Nanjing 211189, China

§ Purple Mountain Laboratories, Nanjing 211111, China

¶ Department of Electrical and Electronic Engineering, The University of Hong Kong, Hong Kong, China

|| Department of Electrical and Electronic Engineering, University of Manchester, Manchester, UK

Emails: {dianxin.luan, john.thompson}@ed.ac.uk, 23578751@student.gla.ac.uk

{j.huang, chxwang}@seu.edu.cn

linzheng@eee.hku.hk, kaitao.meng@manchester.ac.uk

Abstract—This paper proposes a Mamba-assisted neural network framework incorporating self-attention mechanism to achieve improved channel estimation with low complexity for orthogonal frequency-division multiplexing (OFDM) waveforms, particularly for configurations with a large number of subcarriers. With the integration of customized Mamba architecture, the proposed framework handles large-scale subcarrier channel estimation efficiently while capturing long-distance dependencies among these subcarriers effectively. Unlike conventional Mamba structure, this paper implements a bidirectional selective scan to improve channel estimation performance, because channel gains at different subcarriers are non-causal. Moreover, the proposed framework exhibits relatively lower space complexity than transformer-based neural networks. Simulation results tested on the 3GPP TS 36.101 channel demonstrate that compared to other baseline neural network solutions, the proposed method achieves improved channel estimation performance with a reduced number of tunable parameters.

Index Terms—Channel estimation, mamba, attention mechanism, neural networks, orthogonal frequency division multiplexing (OFDM).

I. INTRODUCTION

For sixth generation (6G) communication systems, orthogonal frequency-division multiplexing (OFDM) is expected to continue to serve as baseband modulator [1]–[4]. Therefore, acquiring accurate channel state information (CSI) is essential as it ensures effective compensation for channel impairments, supports high data rate and reliable connectivity. Conventional approaches, such as least squares (LS) and minimum mean squared error (MMSE) [5], [6], cannot meet current demands. The LS estimator has poor performance, whereas the MMSE method, despite its theoretical optimality, relies on actual channel information that is unavailable in the real world. In addition, precise interpolation for doubly-selective channels is usually challenging because statistical models are inaccurate and difficult to handle [7], especially for channel estimates at the data OFDM symbols. These drawbacks highlight the necessity of alternative solutions. Therefore, artificial intelligence (AI) solutions are attracting significant attention due to

their ability to achieve superior performance under complex propagation conditions [8]–[15].

Unlike conventional methods that emphasize closed-form expressions, neural networks aim for locally optimal solutions, such as ChannelNet [16] and ReEsNet [17]. However, neural networks suffer from significant degradation on new channels. To fine-tune neural networks online, the paper [18] proposes a continuous learning-based channel estimation scheme that preserves historical knowledge and achieve an ongoing process of self-improvement. Moreover, the paper [19] proposes federated collaborative learning with pruned-data aggregation to reduce the frequency of online adaptation. To achieve robust generalization, our works [20], [21] proposes design criteria to generate synthetic training datasets that ensure trained channel estimation neural networks perform robustly on previously unseen channels. With the attention-based architecture released in [22], the paper [23], [24] proposes an attention-based channel estimator with a pilot switch network that adapts configurations to channel conditions, balancing accuracy and overhead. An efficient parallel Transformer is proposed in [12] to achieve efficient channel estimation by considering estimation time for reconfigurable intelligent surface (RIS)-aided wireless communication. Our prior studies [25], [26] also propose an encoder–decoder architecture that leverages the transformer encoder to achieve input sparsity according to their relative importance. However, although transformer-based neural networks achieve improved performance, their computational and spatial complexities increase rapidly with the number of OFDM subcarriers due to the larger input sequence length. This will result in high computational consumption, challenging battery-powered handset devices.

In this paper, we propose a mamba-assisted neural network for channel estimation, which deploys a customized mamba block for efficient large-scale subcarriers process. Moreover, we apply a bidirectional state scan to enable the customized Mamba structure capture correlation information from the adjacent two sides, thereby achieving improved performance

and a reduced number of tunable parameters. Experiments tested on 3GPP TS 36.101 channel show that, the proposed method achieves improved channel estimation performance and requires fewer tunable parameters for large number of subcarriers, compared to other neural networks.

II. SYSTEM ARCHITECTURE

A. Baseband and channel settings

This paper considers single antenna transmission for an OFDM cellular system with a frequency spacing of f_{space} at carrier frequency f_r . The randomly generated source signal \mathbf{s} is processed by a Quadrature Phase Shift Keying (QPSK) modulator. The QPSK modulated symbols are assigned to the data subcarriers in the slot. Each slot consists of N_f subcarriers and N_s OFDM symbols. By following the 5G NR specifications in 3GPP TS 38.211, the employed demodulation reference signal (DM-RS) pattern is a single-symbol DM-RS with three additional positions as the default pilot pattern. The 3rd, 6th, 9th and 12th OFDM symbols are reserved for pilots ($N_{pilot} = 4$). For each pilot OFDM symbol, the second subcarriers of each indices of $L_s = 4$ subcarriers is reserved for pilot subcarriers. The pilot signals are assigned by a fixed value, and the vacant pilot subcarriers are set to 0. The inverse fast Fourier transform converts the slot signal into the time domain. Normally the fast Fourier transform (FFT) and inverse fast Fourier transform (IFFT) operators use scaling factors of 1 and $1/N_f$, but those are changed to $1/\sqrt{N_f}$ to avoid changing the power of their outputs. Then the Cyclic-Prefix (CP, of length L_{CP} samples) is added to the front of each symbol to resist the multipath fadings. The channel is assumed to be a multipath channel with M paths which has an impulse response of

$$h(\tau, t) = \sum_{m=0}^{M-1} a_m(t) \delta(\tau - \tau_m T_s) \quad (1)$$

where $a_m(t) = a_m e^{-j2\pi f_{D,m} t + \phi_{D,m}}$ is the path gain of the m th path, τ_m is the corresponding delay normalized by the sampling period T_s , $f_{D,m}$ is the corresponding Doppler shifts and $\phi_{D,m}$ is the corresponding initial phase. Therefore, the n th sampled time-domain $\mathbf{h}(n; t)$ is

$$\mathbf{h}(n; t) = \sum_{m=0}^{M-1} a_m(t) e^{-j\pi \frac{n+(N_f-1)\tau_m}{N_f}} \frac{\sin(\pi \tau_m)}{\sin(\frac{\pi}{N_f}(\tau_m - n))}. \quad (2)$$

For the propagation channel model, this paper uses the Extended Typical Urban (ETU) channel from 3GPP TS 36.101 document, which represents a high delay spread environment. Then the sampled time-domain received signal \mathbf{y} is given by

$$\mathbf{y} = \mathbf{h} \otimes \mathbf{x} + \mathbf{n} \quad (3)$$

where \otimes denotes the convolution operation, \mathbf{n} is assumed to be additive white Gaussian noise (AWGN) and \mathbf{x} is the transmitted time-domain OFDM signal. Each slot is assigned a new channel realization. After removing the CP, the receiver converts the time-domain data to the frequency-domain using

the FFT operation. By assuming that $\forall \tau_m \leq L_{CP}$, the channel gain at the k th subcarrier is

$$\mathbf{H}(k, l) \frac{1}{\sqrt{N_f}} \sum_{m=0}^{M-1} a_m e^{-j2\pi(f_{D,m} T_o l + \phi_{D,m} + \frac{k\tau_m}{N_f})}. \quad (4)$$

for $k = [0, N_f - 1]$ and T_o is one complete OFDM symbol period including the CP. The received signal at k th subcarrier and l th OFDM symbol, $\mathbf{Y}(k, l)$, is of the form:

$$\mathbf{Y}(k, l) = \mathbf{H}(k, l) \mathbf{X}(k, l) + \mathbf{N}(k, l) \quad (5)$$

where $\mathbf{N} \sim \mathcal{CN}(\mathbf{0}, \sigma_N^2 \mathbf{I}_{N_f})$, and complete $\mathbf{H} \in \mathbb{C}^{N_f \times N_s}$ is the channel matrix to be estimated and $\sigma_X^2 = E\{(N_f N_s)^{-1} \|\mathbf{X}\|_F^2\}$. The received pilot signal is then extracted to provide a reference for the channel matrix of each packet. The recovered signal will be filtered to remove the channel effects, and then processed in a QPSK demodulator to obtain the received bit-level data estimates $\hat{\mathbf{s}}$.

B. Conventional methods and baseline neural networks

The LS estimate at the k th subcarrier is given by

$$\hat{\mathbf{H}}_{\text{ls}}(k) = Y_k X_k^{-1}, \quad (6)$$

where Y_k and X_k denote the received and transmitted pilot signals for the k th subcarrier, respectively. This paper applies linear interpolation on $\hat{\mathbf{H}}_{\text{ls}}^{\text{pilot}} \in \mathbb{C}^{\frac{N_f}{L_s} \times N_{\text{pilot}}}$ (LS estimate at the pilot positions) to predict the complete channel matrix. By utilizing exactly actual channel information for improved estimate performance, the linear MMSE estimate for one OFDM symbol $\hat{\mathbf{H}}_{\text{MMSE}} \in \mathbb{C}^{N_f}$ is computed by

$$\hat{\mathbf{H}}_{\text{MMSE}} = \mathbf{R}_{\mathbf{H}_c \mathbf{H}_p} \left(\mathbf{R}_{\mathbf{H}_p \mathbf{H}_p} + \left(\frac{\sigma_N^2}{\sigma_X^2} \right) \mathbf{I}_{N_f} \right)^{-1} \hat{\mathbf{H}}_{\text{ls}} \quad (7)$$

where $\mathbf{H}_c \in \mathbb{C}^{N_f}$ is the actual channel matrix for each OFDM symbol and $\mathbf{H}_p \in \mathbb{C}^{\frac{N_f}{L_s}}$ is the actual channel matrix at the corresponding pilot subcarriers, which are computed by

$$\mathbf{R}_{\mathbf{H}_c \mathbf{H}_p} = \mathbb{E}\{\mathbf{H}_c \mathbf{H}_p^H\}, \mathbf{R}_{\mathbf{H}_p \mathbf{H}_p} = \mathbb{E}\{\mathbf{H}_p \mathbf{H}_p^H\}. \quad (8)$$

These matrices are substituted into Eq. (7) to calculate the $\hat{\mathbf{H}}_{\text{MMSE}}^{\text{pilot}} \in \mathbb{C}^{N_f \times N_{\text{pilot}}}$. $\hat{\mathbf{H}}_{\text{MMSE}}^{\text{pilot}}$ is then interpolated linearly to obtain the estimate for the complete slot. To evaluate performance, InterpolateNet [27], HA02 [25] and Channelformer [26] are implemented as baseline neural networks. InterpolateNet is a low-complexity convolutional neural network with skip connections that only has 9,442 tunable parameters. Both HA02 and Channelformer exploit sub-channel correlations among the input features for improvement.

III. MAMBA-NET: MAMBA-ASSISTED FRAMEWORK

We propose a Mamba-assisted framework (called MambaNet) for channel estimation, as shown in Fig. 1. It implements the multi-head attention mechanism to capture the correlation among the LS input, and then uses a customized Mamba structure to efficiently propagate and refine the channel correlation information over a very large number of subcarriers

(large N_f), leading to both improved performance and reduced complexity.

For the input of MambaNet, the $\hat{\mathbf{H}}_{\text{LS}}^{\text{pilot}} \in \mathbb{C}^{\left(\frac{N_f}{L_s}\right) \times N_{\text{pilot}}}$ is concatenated to be one column vector $\in \mathbb{C}^{\frac{N_f}{L_s} N_{\text{pilot}}}$. The real and imaginary parts of this vector are split into two channels as the second dimension with a size of $\mathbb{R}^{\left(\frac{N_{\text{pilot}} N_f}{L_s}\right) \times 2}$ to form the channel tokenization. The MambaNet is trained by the complete channel matrix $\in \mathbb{R}^{N_f \times N_s \times 2}$ where the second dimension stores the real and imaginary part of the complex channel matrix for the slot.

A. Attention-assisted Mamba module

To ensure neural networks effectively capture the correlation among different subcarriers and OFDM symbols, it consists of two parts which are self-attention module and Mamba module. The first fully-connected layer of the multi-head attention module resizes the LS input $\in \mathbb{R}^{\left(\frac{N_{\text{pilot}} N_f}{L_s}\right) \times 2}$ to $\in \mathbb{R}^{\left(\frac{3N_{\text{pilot}} N_f}{L_s}\right) \times 2}$ by a linear projection

$$\mathbf{y} = \mathbf{Wx} + \mathbf{b} \quad (9)$$

where $\mathbf{W} \in \mathbb{R}^{\left(\frac{3N_{\text{pilot}} N_f}{L_s}\right) \times \left(\frac{N_{\text{pilot}} N_f}{L_s}\right)}$, $\mathbf{b} \in \mathbb{R}^{\left(\frac{3N_{\text{pilot}} N_f}{L_s}\right) \times 1}$ are tunable parameters. Multi-head attention equally splits that to obtain \mathbf{K} , \mathbf{Q} and $\mathbf{V} \in \mathbb{R}^{\left(\frac{N_f}{L_s}\right) \times 2 \times N_{\text{head}}}$ for $N_{\text{head}} = N_{\text{pilot}}$ heads. For each head, the scaled dot-product attention $\mathbf{Y}_{\text{Attention}} \in \mathbb{R}^{\left(\frac{N_f}{L_s}\right) \times 2 \times N_{\text{heads}}}$ [22] is computed by

$$\mathbf{Y}_{\text{Attention}} = \text{softmax} \left(\frac{\mathbf{Q}\mathbf{K}^T}{\sqrt{\frac{N_f}{L_s}}} \right) \mathbf{V}. \quad (10)$$

After concatenating the scaled dot-product attention for each head in the first dimension, the concatenated result $\in \mathbb{R}^{\left(\frac{N_f N_{\text{heads}}}{L_s}\right) \times 2}$ is then processed by a fully-connected layer to generate the output $\in \mathbb{R}^{\left(\frac{N_f N_{\text{heads}}}{L_s}\right) \times 2}$. The layer normalization module then transformed the superimposed result $x \in \mathbb{R}^{\left(\frac{N_f N_{\text{pilot}}}{L_s}\right) \times 2}$ of this output and the neural network input, to obtain the output of the multi-head attention $y \in \mathbb{R}^{\left(\frac{N_f N_{\text{pilot}}}{L_s}\right) \times 2}$, by

$$\mathbf{y} = \mathbf{w} \left(\frac{\mathbf{x} - \mu}{\sqrt{\sigma_x^2 + \varepsilon}} \right) + \mathbf{b} \quad (11)$$

where μ is the mean value of the input \mathbf{x} and σ_x^2 is the corresponding variance, $\varepsilon = 10^{-5}$ to avoid zero-division and $\mathbf{w}, \mathbf{b} \in \frac{N_{\text{pilot}} N_f}{L_s} \times 1$ are the tunable parameters.

We adopt a modified Mamba module operating on the multi-head attention output $\in \mathbb{R}^{\left(\frac{N_f N_{\text{pilot}}}{L_s}\right) \times 2}$ to further propagate channel correlations across a large number of subcarriers with low complexity. The Mamba module is based on the selective space state model (SSM) consists of two main components: gate coefficients generation for dynamic control and selective state scan for state updates. Let the input of mamba block be denoted as $\mathbf{X}^{\text{mamba}} \in \mathbb{R}^{\left(\frac{N_{\text{pilot}} N_f}{L_s}\right) \times 2}$, where the first

dimension corresponds to the effective sequence length of the attention signals and the second dimension denotes the channel dimension. A fully connected layer is first applied to increase the channel dimension of $\mathbf{X}^{\text{mamba}}$ from $\mathbb{R}^{\left(\frac{N_{\text{pilot}} N_f}{L_s}\right) \times 2}$ to $\mathbb{R}^{\left(\frac{N_{\text{pilot}} N_f}{L_s}\right) \times 2C_{\text{spread}}}$ where $C_{\text{spread}} = 24$, and then split this output to two sub-matrix $\mathbf{U}_{\text{main}} \in \mathbb{R}^{\left(\frac{N_{\text{pilot}} N_f}{L_s}\right) \times C_{\text{spread}}}$ and $\mathbf{U}_{\text{gate}} \in \mathbb{R}^{\left(\frac{N_{\text{pilot}} N_f}{L_s}\right) \times C_{\text{spread}}}$.

1) *Gate coefficients generation:* To calculate the gate coefficients, instead of using depthwise convolution, a fully-connected layer is applied to \mathbf{U}_{main} to obtain $\mathbf{X}_{\mathbf{c}} \in \mathbb{R}^{\left(\frac{N_{\text{pilot}} N_f}{L_s}\right) \times C_{\text{spread}}}$. The reason is that the input LS estimate are inherently non-causal, resulting the subsequent in-process features remain non-causal. This indicates that fully-connected layer is an optimum option for this data type. Then the silu layer is applied to $\mathbf{X}_{\mathbf{c}} \in \mathbb{R}^{\left(\frac{N_{\text{pilot}} N_f}{L_s}\right) \times C_{\text{spread}}}$, defined as

$$\mathbf{X}_{\mathbf{dc}} = \text{silu}(\mathbf{X}_{\mathbf{c}}) = \frac{\mathbf{X}_{\mathbf{c}}}{1 + e^{-\mathbf{X}_{\mathbf{c}}}}. \quad (12)$$

The $\mathbf{X}_{\mathbf{dc}} \in \mathbb{R}^{\left(\frac{N_{\text{pilot}} N_f}{L_s}\right) \times C_{\text{spread}}}$ is then projected into three branches to generate the gate coefficients $\mathbf{a}, \mathbf{b}, \mathbf{g} \in \mathbb{R}^{\left(\frac{N_{\text{pilot}} N_f}{L_s}\right) \times C_{\text{spread}}}$ by

$$\mathbf{a} = \sigma(\mathbf{X}_{\mathbf{dc}} \mathbf{W}_{\mathbf{a}} + \mathbf{b}_{\mathbf{a}}), \mathbf{W}_{\mathbf{a}} \in \mathbb{R}^{24 \times 24}, \mathbf{b}_{\mathbf{a}} \in \mathbb{R}^{24}, \quad (13)$$

$$\mathbf{b} = \mathbf{X}_{\mathbf{dc}} \mathbf{W}_{\mathbf{b}} + \mathbf{b}_{\mathbf{b}}, \mathbf{W}_{\mathbf{b}} \in \mathbb{R}^{24 \times 24}, \mathbf{b}_{\mathbf{b}} \in \mathbb{R}^{24}, \quad (14)$$

$$\mathbf{g} = \text{silu}(\mathbf{U}_{\text{gate}} \mathbf{W}_{\mathbf{g}} + \mathbf{b}_{\mathbf{g}}), \mathbf{W}_{\mathbf{g}} \in \mathbb{R}^{24 \times 24}, \mathbf{b}_{\mathbf{g}} \in \mathbb{R}^{24}, \quad (15)$$

where $\sigma(\cdot) = \frac{1}{1+e^{-x}}$ is the sigmoid activation.

2) *Bidirectional selective state space scan:* The coefficients \mathbf{a}, \mathbf{b} are used to calculate the scan recurrence for state updates selectively. Because the channel gain elements are non-causal, a backward scan are deployed to effectively capture the non-causal correlation rather than only performing a forward scan. For each step $t = \left[1, \frac{N_{\text{pilot}} N_f}{L_s}\right]$, the hidden state $\mathbf{h}_t \in \mathbb{R}^{1 \times C_{\text{spread}}}$ is given by

$$\text{Forward: } \mathbf{h}_t^f = \mathbf{a}_t \circ \mathbf{h}_{t-1}^f + \mathbf{b}_t, \quad \mathbf{h}_0^f = \mathbf{0}, \quad (16)$$

$$\text{Backward: } \mathbf{h}_t^b = \mathbf{a}_t \circ \mathbf{h}_{t+1}^b + \mathbf{b}_t, \quad \mathbf{h}_{\left(\frac{N_{\text{pilot}} N_f}{L_s} + 1\right)}^b = \mathbf{0}, \quad (17)$$

$$\text{Overall: } \mathbf{h}_t = \mathbf{h}_t^f + \mathbf{h}_t^b. \quad (18)$$

where $\mathbf{a}_t, \mathbf{b}_t$ are the t th row of \mathbf{a}, \mathbf{b} and the operator \circ denotes the Hadamard product. As shown in Eq. (16) and Eq. (17), the coefficient \mathbf{a} controls the degree to which the adjacent hidden state is preserved. A higher value of \mathbf{a} retains more information of the adjacent hidden states, while a lower value accelerates forgetting. The coefficient \mathbf{b} provides an additive contribution that injects new information from the current input into the

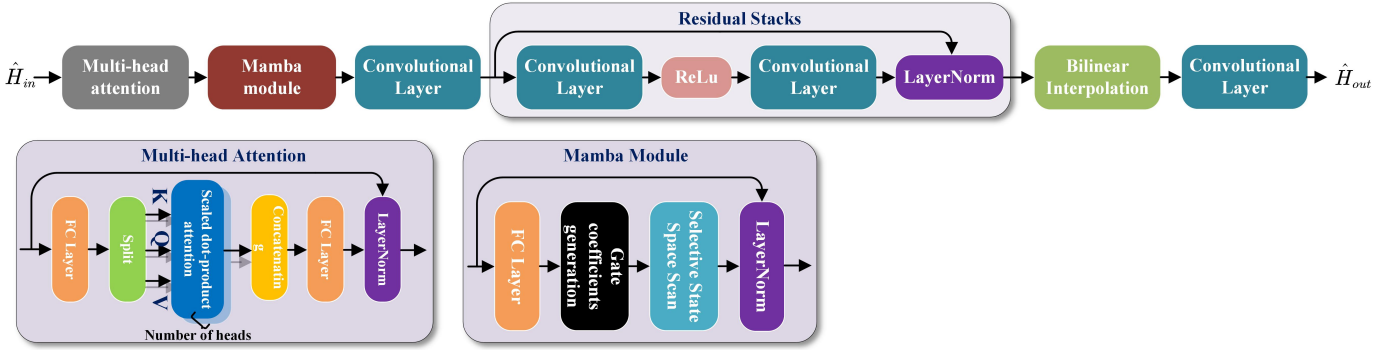


Fig. 1. MambaNet: Mamba-assisted framework with self-attention mechanism. It involves an attention-assisted Mamba block and a residual convolutional neural network.

state update. To compute this recurrence efficiently, Eq. (18) is equivalently expressed in parallel form as

$$\mathbf{H}_t^f = \left(\prod_{i=1}^t \mathbf{a}_i \right) \sum_{i=1}^t \frac{\mathbf{b}_i}{\prod_{j=1}^i \mathbf{a}_j}, \quad (19)$$

$$\mathbf{H}_t^b = \left(\prod_{i=1}^t \mathbf{a}_i \right) \sum_{i=1}^t \frac{\mathbf{b}_i}{\prod_{j=i}^t \mathbf{a}_j}, \quad (20)$$

$$\mathbf{H}_t^{\text{mamba}} = \mathbf{H}_t^f + \mathbf{H}_t^b, \quad (21)$$

leading to stacked states $\mathbf{H}^{\text{mamba}} \in \mathbb{R}^{\left(\frac{N_{\text{pilot}}N_f}{L_s}\right) \times C_{\text{spread}}}$ for the entire step t . The gate control signal \mathbf{g} modulates the entire \mathbf{H} and determines the extent to which the internal state contributes to the output. This output is then projected to obtain the mamba output $\mathbf{Y}^{\text{mamba}} \in \mathbb{R}^{\left(\frac{N_{\text{pilot}}N_f}{L_s}\right) \times 2}$, which is given by

$$\mathbf{Y}^{\text{mamba}} = (\mathbf{g} \circ \mathbf{H}) \mathbf{W}_{\text{out}} + \mathbf{b}_{\text{out}} \quad (22)$$

where $\mathbf{W}_{\text{out}} \in \mathbb{R}^{C_{\text{spread}} \times 2}$, $\mathbf{b}_{\text{out}} \in \mathbb{R}^2$ are tunable parameters. Then layer normalization is applied to the superimposed results of the mamba input $\mathbf{X}^{\text{mamba}} \in \mathbb{R}^{\left(\frac{N_{\text{pilot}}N_f}{L_s}\right) \times 2}$ and the mamba output $\mathbf{Y}^{\text{mamba}} \in \mathbb{R}^{\left(\frac{N_{\text{pilot}}N_f}{L_s}\right) \times 2}$ to form the output of attention-assisted Mamba module $\mathbf{Y}_a \in \mathbb{R}^{\left(\frac{N_{\text{pilot}}N_f}{L_s}\right) \times 2}$.

For time complexity of this mamba module, linear projections operate on the channel dimension, while the temporal dependencies are modeled entirely through the selective scan along the sequence length (first dimension). The resulting complexity is $\mathcal{O}\left(\frac{N_{\text{pilot}}N_f}{L_s}\right)$, which is substantially lower than the $\mathcal{O}\left(\left(\frac{N_{\text{pilot}}N_f}{L_s}\right)^2\right)$ complexity of self-attention. Therefore, the mamba module has the capability to model long-range dependencies efficiently, especially when the N_f is very large or the in-processing features of the previous multi-head attention module have a large sequence length.

B. Residual architecture with up-sampling modules

To achieve the precise channel estimate for the complete slot, the in-processing features $\mathbf{Y}_a \in \mathbb{R}^{\left(\frac{N_{\text{pilot}}N_f}{L_s}\right) \times 2}$ are

reshaped to $\mathbb{R}^{\left(\frac{N_f}{L_s}\right) \times N_{\text{pilot}} \times 2}$. This enlarges the effective receptive field compared to the previous sequence features, which should improve the performance of residual architecture on super-resolution. The first convolutional layer has 12 filters with a kernel size of $5 \times 5 \times 2$ followed by a stack of seven residual blocks. Each residual block consists of one convolutional layer with 12 filters, each corresponding to a kernel size of $5 \times 5 \times 12$, followed by one ReLU layer and one convolutional layer with 12 filters and the kernel size of each is $5 \times 5 \times 12$. The layer normalization processes the superimposed result of the input and output of the final residual block to the upsampling module.

This paper exploits bilinear interpolation as up-sampling function, which resizes the output $\in \mathbb{R}^{\frac{N_f}{L_s} \times N_{\text{pilot}} \times 12}$ from the previous residual stacks to a size of $\mathbb{R}^{N_f \times N_s \times 12}$. The last coupled convolutional layer has 2 filters with the kernel size of 96×5 to generate the output $\in \mathbb{R}^{N_f \times N_s \times 2}$.

IV. SIMULATIONS

MSE is a key performance metric that evaluates the distance between the actual channel matrix and the estimate, which is defined as

$$\text{MSE}(\hat{\mathbf{H}}, \mathbf{H}) = (N_f N_s)^{-1} \mathbb{E} \left\{ \left\| \hat{\mathbf{H}} - \mathbf{H} \right\|_F^2 \right\}. \quad (23)$$

The bit error ratio (BER) is another metric defined as the ratio of mismatch between the $\hat{\mathbf{s}}$ and \mathbf{s} . The hyper-parameters of system configuration are given in Table I. For training procedure, the training dataset is generated on the ETU channel which consists of 125,000 independent channel samples (95% for training and 5% for validation). The SNR range is from 5 dB to 25 dB and the $f_{D,\text{max}}$ is from 0 Hz to 97 Hz. The loss function for InterpolateNet is the MSE loss, and for the Channelformer, HA02 and proposed method is the Huber loss given in [26]. To average out Monte Carlo effects, each sample of the simulation curves is tested with 5,000 independent channel realizations.

A. MSE and BER performance over an extended SNR range

We evaluate the MSE and BER performance on the ETU channel over an extended SNR range to investigate the robust-

TABLE I
SIMULATION HYPER-PARAMETERS

Offline-training hyper-parameters		Baseband hyper-parameters	
Optimizer	Adam	N_f	228
Maximum epoch	100	N_s	14
Initial learning rate (lr)	0.0005	L_{CP}	12
Drop period for lr	25	f_r	5.0 GHz
Drop factor for lr	0.5	$f_{D,max}$	97 Hz
Minibatch size	128	f_{space}	15 kHz
L2 regularization	10^{-7}	SNR range	from 5 dB to 30 dB

ness capability. The extended SNR range is from 5 dB to 30 dB and maximum Doppler shift is from 0 Hz to 97 Hz.

Fig. 2a provides the MSE performance for each method over the SNR range from 5 dB to 30 dB. Compared with LS estimate, the MambaNet significantly improves the performance which also outperforms InterpolateNet, HA02 and Channelformer for the whole SNR range. For InterpolateNet, the corresponding MSE varies from 0.0013 to 0.0203 which is worse than other neural network solutions. Compared with HA02 and Channelformer, the MSE of MambaNet decreases by 0.00072 and 0.000065 for 30dB SNR respectively. Moreover, MambaNet outperforms the MMSE method at 30dB SNR, while MMSE requires exact channel information to precisely predict the complete channel matrix. These results demonstrate the effectiveness and practicality of the customized Mamba block, whose bidirectional selective state scan enables long-range propagation of element-wise correlation information, allowing MambaNet to achieve superior estimation performance compared with other solutions.

Fig. 2b compares the BER performance of each method over this extended SNR range, where the MambaNet achieves the best performance. At 5 dB SNR point, MambaNet achieves 0.0057 BER while Channelformer has a BER value of 0.0058. The corresponding BER values for InterpolateNet and HA02 are 0.0064 and 0.0060 respectively. The BER values at 30 dB SNR are 0.00023 for HA02, 0.00021 for InterpolateNet and 0.00019 for Channelformer respectively. MambaNet achieves a very low BER of 0.00018 while MMSE method only achieves a BER of 0.00022. For the high SNR range, neural network solutions can outperform the MMSE method because this paper uses linear interpolation for the MMSE method to obtain the complete channel prediction.

B. Complexity analysis

We also compare the computational complexity of the proposed method and the baseline neural network methods. With increasing N_f , the total number of tunable parameters for MambaNet scales as $\mathcal{O}\left(\left(\frac{N_f N_{pilot}}{L_s}\right)^2\right)$. However, for Channelformer and HA02, they exhibit a complexity of $\mathcal{O}\left((N_f N_s)^2\right)$ which represents a significant increase compared to MambaNet. Both Channelformer and HA02 have severe parameter explosion with increasing N_f to a very large number. However, the number of parameters for mambaNet increases slowly and has a significant reduction. Compared

with Channelformer and HA02, mambaNet has a 73% and 76% reduction on the number of tunable parameters but requires twice the running time of Channelformer. Although the total number of tunable parameters for interpolateNet is fixed, it shows relatively poor performance in Fig. 2a. Both the number of tunable parameters and the running time normalized by that of LS method for each method are provided in Table II.

TABLE II
COMPLEXITY ANALYSIS

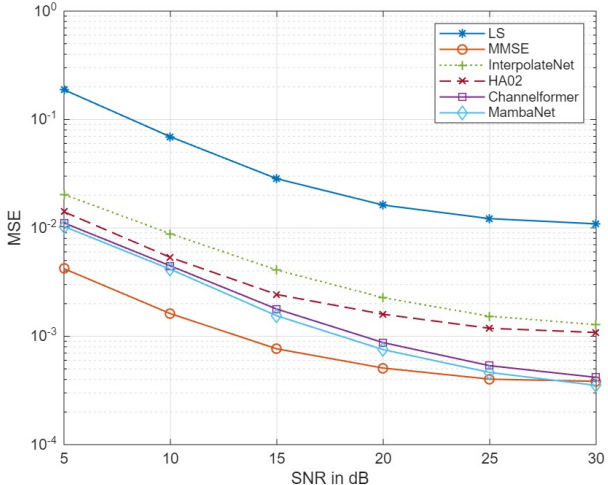
	Tunable parameters	Normalized running time
InterpolateNet	0.01M	12.7
HA02	1.1M	17.2
Channelformer	0.93M	24.5
MambaNet	0.35M	27.3

V. CONCLUSION

In this paper, we propose a mamba-assisted framework to achieve improved channel estimation and reduced space complexity for large-scale subcarrier configuration. It has a customized mamba block to efficiently capture the long-distance element-wise dependencies over a large number of subcarriers. Especially, a bidirectional state scan is employed to enable the Mamba-assisted structure to capture correlation information from both forward and backward directions for the non-causal input features. Experiments tested on 3GPP TS 36.101 channel show that MambaNet achieves improved channel estimation performance and requires fewer tunable parameters as the number of subcarriers increases, compared to other transformer-based baseline neural networks.

REFERENCES

- [1] C.-X. Wang, X. You, X. Gao, X. Zhu, Z. Li, C. Zhang, H. Wang, Y. Huang, Y. Chen, H. Haas *et al.*, “On the road to 6g: Visions, requirements, key technologies, and testbeds,” *IEEE Communications Surveys & Tutorials*, vol. 25, no. 2, pp. 905–974, 2023.
- [2] Q. Wu, B. Zheng, C. You, L. Zhu, K. Shen, X. Shao, W. Mei, B. Di, H. Zhang, E. Basar *et al.*, “Intelligent surfaces empowered wireless network: Recent advances and the road to 6g,” *Proceedings of the IEEE*, 2024.
- [3] H. Lu, Y. Zeng, C. You, Y. Han, J. Zhang, Z. Wang, Z. Dong, S. Jin, C.-X. Wang, T. Jiang *et al.*, “A tutorial on near-field xl-mimo communications toward 6g,” *IEEE Communications Surveys & Tutorials*, vol. 26, no. 4, pp. 2213–2257, 2024.
- [4] C.-X. Wang, M. Di Renzo, S. Stanczak, S. Wang, and E. G. Larsson, “Artificial intelligence enabled wireless networking for 5g and beyond: Recent advances and future challenges,” *IEEE Wireless Communications*, vol. 27, no. 1, pp. 16–23, 2020.
- [5] J.-J. Van De Beek, O. Edfors, M. Sandell, S. K. Wilson, and P. O. Borjesson, “On channel estimation in ofdm systems,” in *1995 IEEE 45th Vehicular Technology Conference. Countdown to the Wireless Twenty-First Century*, vol. 2. IEEE, 1995, pp. 815–819.
- [6] O. Edfors, M. Sandell, J.-J. Van de Beek, S. K. Wilson, and P. O. Borjesson, “Ofdm channel estimation by singular value decomposition,” *IEEE Transactions on Communications*, vol. 46, no. 7, pp. 931–939, 1998.
- [7] R. Nissel, F. Ademaj, and M. Rupp, “Doubly-selective channel estimation in FBMC-OQAM and OFDM systems,” in *2018 IEEE 88th Vehicular Technology Conference (VTC-Fall)*. IEEE, 2018, pp. 1–5.
- [8] H. Ye, G. Y. Li, and B.-H. Juang, “Power of deep learning for channel estimation and signal detection in ofdm systems,” *IEEE Wireless Communications Letters*, vol. 7, no. 1, pp. 114–117, 2017.



(a) MSE results of the MambaNet

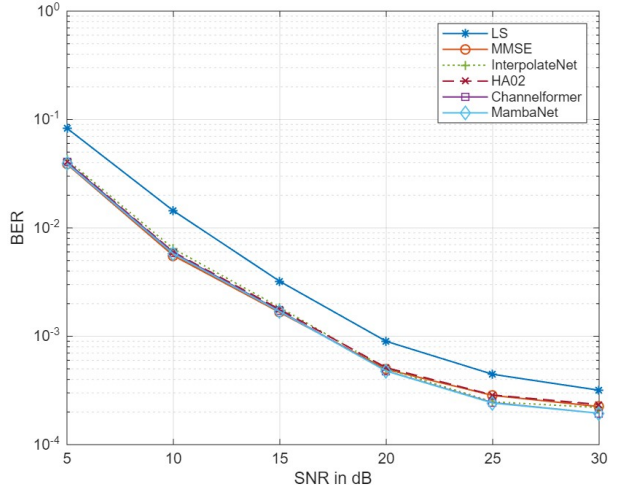


Fig. 2. MSE and BER results for the InterpolateNet, HA02, Channelformer and MambaNet tested on the ETU channel.

[9] D. Neumann, T. Wiese, and W. Utschick, “Learning the MMSE channel estimator,” *IEEE Transactions on Signal Processing*, vol. 66, no. 11, pp. 2905–2917, 2018.

[10] M. Nerini, V. Rizzello, M. Joham, W. Utschick, and B. Clerckx, “Machine learning-based CSI feedback with variable length in fdd massive mimo,” *IEEE Transactions on Wireless Communications*, vol. 22, no. 5, pp. 2886–2900, 2022.

[11] B. Fesl, M. B. F. Strasser, M. Joham, and W. Utschick, “Diffusion-based generative prior for low-complexity mimo channel estimation,” *IEEE Wireless Communications Letters*, 2024.

[12] J. Guo, G. Liu, Q. Wu, and P. Fan, “Parallel attention-based transformer for channel estimation in ris-aided 6g wireless communications,” *IEEE Transactions on Vehicular Technology*, 2024.

[13] J. Wang, X. Mei, J. Xiao, X. Li, P. Zhu, A. Nallanathan, and C. Yuen, “Deep learning based wavenumber domain channel estimation for holographic mimo communications,” *IEEE Transactions on Vehicular Technology*, pp. 1–6, 2025.

[14] D. Luan and J. Thompson, “Robust channel estimation for optical wireless communications using neural network,” *IEEE Wireless Communications Letters*, pp. 1–1, 2026.

[15] W. Yuan, F. Liu, C. Masouros, J. Yuan, D. W. K. Ng, and N. González-Prelcic, “Bayesian predictive beamforming for vehicular networks: A low-overhead joint radar-communication approach,” *IEEE Transactions on Wireless Communications*, vol. 20, no. 3, pp. 1442–1456, 2020.

[16] M. Soltani, V. Pourahmadi, A. Mirzaei, and H. Sheikhzadeh, “Deep learning-based channel estimation,” *IEEE Communications Letters*, vol. 23, no. 4, pp. 652–655, 2019.

[17] L. Li, H. Chen, H.-H. Chang, and L. Liu, “Deep residual learning meets ofdm channel estimation,” *IEEE Wireless Communications Letters*, vol. 9, no. 5, pp. 615–618, 2019.

[18] L. Kong, X. Liu, X. Zhang, J. Xiong, H. Zhao, and J. Wei, “Representation-based continual learning for channel estimation in dynamic wireless environments,” *IEEE Transactions on Wireless Communications*, 2025.

[19] S. Wang, T. Wang, and X. Wang, “Fedpda: Collaborative learning for reducing online-adaptation frequency of neural receivers,” in *IEEE INFOCOM 2025-IEEE Conference on Computer Communications*. IEEE, 2025, pp. 1–10.

[20] D. Luan and J. Thompson, “Achieving robust generalization for wireless channel estimation neural networks by designed training data,” in *ICC 2023-IEEE International Conference on Communications*. IEEE, 2023, pp. 3462–3467.

[21] ———, “Achieving robust channel estimation neural networks by designed training data,” *IEEE Transactions on Cognitive Communications and Networking*, 2025.

[22] A. Vaswani, N. Shazeer, N. Parmar, J. Uszkoreit, L. Jones, A. N. Gomez, Ł. Kaiser, and I. Polosukhin, “Attention is all you need,” *Advances in neural information processing systems*, vol. 30, 2017.

[23] F. Liu, J. Zhang, P. Jiang, C.-K. Wen, and S. Jin, “CE-VIT: A robust channel estimator based on vision transformer for ofdm systems,” in *GLOBECOM 2023-2023 IEEE Global Communications Conference*. IEEE, 2023, pp. 4798–4803.

[24] F. Liu, P. Jiang, J. Zhang, W. Wang, C.-K. Wen, and S. Jin, “Pd-cevit: A novel pilot pattern design and channel estimation network for ofdm systems,” *IEEE Transactions on Communications*, 2024.

[25] D. Luan and J. Thompson, “Attention based neural networks for wireless channel estimation,” in *2022 IEEE 95th Vehicular Technology Conference:(VTC2022-Spring)*. IEEE, 2022, pp. 1–5.

[26] D. Luan and J. S. Thompson, “Channelformer: Attention based neural solution for wireless channel estimation and effective online training,” *IEEE Transactions on Wireless Communications*, vol. 22, no. 10, pp. 6562–6577, 2023.

[27] D. Luan and J. Thompson, “Low complexity channel estimation with neural network solutions,” in *WSA 2021; 25th International ITG Workshop on Smart Antennas*. VDE, 2021, pp. 1–6.